Atmos. Chem. Phys. Discuss., 13, 30687–30720, 2013
www.atmos-chem-phys-discuss.net/13/30687/2013/
doi:10.5194/acpd-13-30687-2013

Atmospheric Chemistry and Physics Discussions

Impact of biomass burning on haze pollution in the Yangtze River Delta, China: a case study in summer 2011

Z. Cheng[1], S. Wang[1,2], X. Fu[1], J. G. Watson[3,8], J. Jiang[1,2], Q. Fu[4], C. Chen[5], B. Xu[6], J. Yu[7], J. C. Chow[3,8], and J. Hao[1,2]

[1]School of Environment, and State Key Joint Laboratory of Environment Simulation and Pollution Control, Tsinghua University, Beijing 100084, China
[2]State Environmental Protection Key Laboratory of Sources and Control of Air Pollution Complex, Beijing 100084, China
[3]Division of Atmospheric Sciences, Desert Research Institute, 2215 Raggio Parkway, Reno, NV 89512, USA
[4]Shanghai Environmental Monitoring Center, Shanghai 200030, China
[5]Shanghai Academy of Environmental Sciences, Shanghai 200233, China
[6]Zhejiang Environmental Monitoring Center, Hangzhou 310015, China
[7]Jiangsu Environmental Monitoring Center, Nanjing 210036, China
[8]SKLLQG, Institute of Earth Environment, Chinese Academy of Sciences, Xi'an, 710075, China

Received: 18 August 2013 – Accepted: 31 October 2013 – Published: 25 November 2013

Correspondence to: S. Wang (shxwang@tsinghua.edu.cn)

Published by Copernicus Publications on behalf of the European Geosciences Union.

ACPD
13, 30687–30720, 2013

Abstract

Open biomass burning is an important source of air pollution in China and globally. Joint observations of air pollution were conducted in five cities (Shanghai, Hangzhou, Ningbo, Suzhou and Nanjing) of the Yangtze River Delta, and a heavy haze episode with visibility 2.9–9.8 km was observed from 28 May to 6 June 2011. The contribution of biomass burning was quantified using both ambient monitoring data and the WRF/CMAQ model simulation. It was found that the average and maximum daily $PM_{2.5}$ concentrations during the episode were 82 $\mu g\,m^{-3}$ and 144 $\mu g\,m^{-3}$, respectively. Weather pattern analysis indicated that a stagnant process enhanced the accumulation of air pollutants, while the following precipitation process scavenged the pollution. Daily minimum mixing depth during the stagnant period was below 50 m. Both observation data and CMAQ model simulation indicated that biomass open burning contributed 37 % of $PM_{2.5}$, 70 % of organic carbon and 61 % of elemental carbon. Satellite-detected fire spots, back-trajectory analysis and air model simulation can be integrated to identify the locations where the biomasses are burned. The results also suggest that the impact of biomass open burning is regional, due to the substantial inter-province transport of air pollutants. These findings would improve the understanding of not only heavy haze and air pollution episodes, but also the emissions of such open fires.

1 Introduction

Emissions from biomass open burning have significant regional and global impacts on human health, visibility, and climate (Crutzen and Andreae, 1990; Penner et al., 1992; Watson, 2002). In eastern China, large amounts of crop residues are burned in the field during the post-harvest seasons (i.e., May–June and October–November) (Streets et al., 2003; Yan et al., 2006). The open burning of biomass could cause severe air pollution and haze issue in a large region from the Pearl River Delta (PRD) to the Yangtze River Delta (YRD) and Beijing–Tianjin–Hebei (Wang et al., 2007; Li et

ACPD
13, 30687–30720, 2013

al., 2010; Zhang et al., 2010; Zhu et al., 2010; Yin et al., 2011; Huang et al., 2012a; Cheng et al., 2013).

The YRD, including seven cities of northern Zhejiang Province, the Shanghai municipality and eight cities of southern Jiangsu Province (as shown in Fig. 1b), is one of the most important regions of eastern China. Heavy industries including petro-chemistry, iron and steel production, and automobile manufacturing drive the YRD economy. In the meanwhile, the YRD is also a large producer of agricultural products, including wheat, rice, corn and cole flowers, resulting in large amounts of crop residue open burned. Previous studies about biomass burning in the YRD mainly focused on either Nanjing (Zhang et al., 2011; Gao et al., 2012; Su et al., 2012; Zhu et al., 2012) or Shanghai (Huang et al., 2012a; Zhang et al., 2011). Since biomass burning was distributed over a large area over the YRD rural regions, its emissions can transport over long distances under decent meteorological conditions (Cheng et al., 2011), implying the necessity for regional joint observation and analysis to investigate the pollutant transport and accumulation.

Furthermore, biomass burning usually exhibited in the forms of prescribed burning or residential wood heating in urban areas of developed countries. For the prescribed burning, the contribution was estimated to vary in 2.8–43 % (0.3–5.1 $\mu g\,m^{-3}$) of the ambient $PM_{2.5}$ (particles with aerodynamic diameters no more than 2.5 µm) load in Australia and the US (Reisen et al., 2013; Tian et al., 2009), while the contribution of residential wood heaters was in the range of 27–77 % (3.2–9.8 $\mu g\,m^{-3}$) of the $PM_{2.5}$ load in winter of the southeastern US and Australia (Reisen et al., 2013; Zhang et al., 2010), as well as 64 % (12.3 $\mu g\,m^{-3}$) of organic carbon (OC) and 11 % (1.8 $\mu g\,m^{-3}$) of elemental carbon (EC) in the winter of Portugal (Gelencsér, 2007). Meanwhile, the biomass burning contribution ratio to ambient $PM_{2.5}$ mass in China was 15–24 % (12–27 $\mu g\,m^{-3}$) (Cheng et al., 2013; Song et al., 2007; Wang et al., 2009) in Beijing and 4–19 % (5.4–25.4 $\mu g\,m^{-3}$) in Guangzhou (Wang et al., 2007). Although the biomass burning contribution ratio to $PM_{2.5}$ in China had no substantial differences from that of the developed countries under the impact of high emissions from transportation and

ACPD
13, 30687–30720, 2013

industry, the absolute biomass burning contributed $PM_{2.5}$ concentrations were much higher than those of developed locations, mostly due to the burning fuel and method as well as the burning intensity. Hence the estimation of the ambient $PM_{2.5}$ contribution from biomass burning during the heavy haze episode was meaningful and important for further pollution control assessment, especially in the absence of the $PM_{2.5}$ contribution estimation in the YRD region.

In this study, joint observations of air pollution were conducted in five cities (Shanghai, Hangzhou, Ningbo, Suzhou and Nanjing) of the YRD. A heavy haze episode with visibility 2.9–9.8 km was observed from 28 May to 6 June 2011. The impacts of meteorological conditions were analyzed. The contribution of biomass burning to $PM_{2.5}$ mass and carbon concentrations were quantified using the method of source markers and air quality model simulations.

2 Materials and methods

2.1 Field observations

Five sampling sites were located in Ningbo and Hangzhou of Zhejiang Province, and Shanghai, Suzhou and Nanjing of Jiangsu Province to represent urban residential and commercial areas (Fig. 1b). These sites were 100–300 km apart to characterize urban-to-regional scale zones of influence (Chow et al., 2002). Site details were given in Table S-1 and discussed in the Supplement. The sampling and analysis methods were documented in Table S-2 and explained in the Supplement. Data used here included the continuous hourly $PM_{2.5}$ and PM_{10} (particles with aerodynamic diameters no more than 10 µm) mass concentrations measured by Tapered Element Oscillating Microbalance (TEOM) at 50 °C, meteorological parameters including relative humidity (RH), temperature, wind speed/direction, and visual range (forward light scattering) for all five sites. Furthermore, daily average concentrations of $PM_{2.5}$ species were obtained

ACPD
13, 30687–30720, 2013

by filter sampling and chemical analysis in the laboratory at the sites of Shanghai, Suzhou and Nanjing.

The TOEM lost some of the volatile particulate matter (PM) at 50 °C (Chow et al., 2008), but comparisons with collocated filters showed that this loss was less than 10–20 % of the gravimetric mass. The Belfort and Vaisala forward scattering devices used for visual range measurement correlated well with the human observations at nearby meteorological stations, with R^2 = 0.73–0.87 and regression slopes of 0.91–1.03. Daily, 22 h (14:00 LST to 12:00 LST on the following day) $PM_{2.5}$ Teflon-membrane and quartz-fiber filter samples were also taken. The mass concentrations of $PM_{2.5}$ and its metal elements, ions and carbonaceous matter were analyzed in the lab, and the detail information was given in the Supplement. Organic matter (OM) was estimated by 1.55 × OC to account for unmeasured hydrogen (H) and oxygen (O) according to HR-ToF-AMS and SP2 measurement in Shanghai (Huang et al., 2012b). Soil was calculated by the weighted summary of five major soil elements, Al, Si, Ca, Fe, and Ti (Lowenthal, 2007). The trace elements consist of the elements measured by X-ray fluorescence (XRF) with the removal of soil elements (Yang et al., 2011). Non-soil potassium (K^+), which was calculated as water-soluble K^+ minus the part of soil that was 0.6*[Fe] (Hand, 2011), could all be regarded as being from biomass burning (Wang et al., 2007).

2.2 Regional meteorology and fire emissions

Mixing depths and precipitation data were obtained from the Global Data Assimilation System (GDAS) model (Rolph, 2013), which was run at 00:00, 06:00, 12:00, and 18:00 UTC and gave the analysis file of current time as well as the forecast file for three hours later. The UTC time was converted to LST time by adding 8 h for Beijing Time in China. Mixing depths correspond to each time, while precipitation was cumulative for 3 h before the indicated time. Mixing depths were verified by comparison with the vertical lidar observation in Shanghai (Huang et al., 2012a). The Hybrid Single-Particle Lagrangian Integrated Trajectory (HYSPLIT) model (Draxler and Rolph, 2013; Rolph,

ACPD
13, 30687–30720, 2013

2013) was run in the back-trajectory mode at 100 m AGL starting at 12:00 LST, and every three hours thereafter, for the previous 24 h.

Active fire locations were obtained from the Fire Information for Resource Management System (FIRMS) derived from the Moderate Resolution Imaging Spectroradiometer (MODIS) (Davies et al., 2009). Daily 500 hPa height and surface weather patterns analysis charts over East Asia were obtained from the Korea Meteorological Administration.

2.3 Receptor modeling for source apportionment

The tracer solution to the Chemical Mass Balance (CMB) receptor model (Watson et al., 2008) was used to estimate the contributions of biomass burning to $PM_{2.5}$ mass concentrations. Biomass burning markers include water-soluble K^+ (Cheng et al., 2013; Duan et al., 2004), levoglucosan (Sullivan et al., 2008; Wang et al., 2007) and black carbon (BC) absorption concentration differences between 330 nm and 88 nm (Wang et al., 2011b). Non-soil water-soluble K^+ was used as the marker of biomass burning, as it is the only marker quantified. The ratios of $PM_{2.5}$/non-soil K^+, OC/non-soil K^+ and EC/non-soil K^+ for biomass burning source profiles were decided according to literature results. Then these ratios were multiplied by the ambient non-soil K^+ levels determined from each $PM_{2.5}$ filter sample to determine the contribution of biomass burning. It shall be noticed that this method only estimated the primary $PM_{2.5}$ or OC contribution emitted directly by biomass burning, and did not include the secondary $PM_{2.5}$ or OC oxidized from the gaseous pollutant emitted by biomass burning.

2.4 WRF/CMAQ model

The Weather Research and Forecasting (WRF) model (version 3.3.1) and Community Multiscale Air Quality (CMAQ) model (version 5.0) were used to simulate the pollution episode. The CMAQ modeling domains were shown in Fig. 1a, while the WRF domain was a 12 km extension in four directions. Fourteen vertical layers were included from

ACPD
13, 30687–30720, 2013

the height of the surface to 100 mbar. The detail model configuration and parameters were given in Fu et al. (2013). The anthropogenic emissions inventory was based on the local energy consumption statistics, and measured emission factors for both China (domains 1 and 2) (Wang et al., 2011a) and the YRD region (domain 3) (Fu et al., 2013). Biomass burning emissions were temporally and spatially allocated according to the detected time and brightness of fire points derived from FIRMS (Davies et al., 2009). Natural biogenic VOCs emissions were generated from the MEGAN model (Guenther et al., 2006).

The contribution of biomass burning to particle concentrations was estimated using sensitivity analyses. The base case included emissions of all sources from all of the five sub-regions, and an additional five runs dropped biomass emissions from each sub-region (as shown in Fig. 1a) in sequence. The difference between the base case $PM_{2.5}$/OC/EC and each of the next five cases provides the contribution from that region to each receptor. The difference summary of all sub-regions was regarded as the total contribution of biomass burning. The receptors here only included the five grids where monitoring sites were located.

3 Results and discussion

3.1 Characteristics of particulate matter pollution

Figure 2 shows hourly PM_{10} and $PM_{2.5}$ mass concentrations from the TEOM during the biomass burning episode. During this episode, daily average PM_{10} concentration of all sites was 124 $\mu g\,m^{-3}$, ranging from 88 (Shanghai) to 151 $\mu g\,m^{-3}$ (Nanjing), while the daily average $PM_{2.5}$ concentration was 82 $\mu g\,m^{-3}$, ranging from 67 (Shanghai) to 98 $\mu g\,m^{-3}$ (Nanjing). The average of the $PM_{2.5}/PM_{10}$ mass ratio during the episode was 66 %, higher than that of northern Chinese cities. The maximum daily average concentrations were 209 $\mu g\,m^{-3}$ for PM_{10} and 144 $\mu g\,m^{-3}$for $PM_{2.5}$, indicating that $PM_{2.5}$ is the major cause of this haze event. The peak daily concentrations occurred on

ACPD
13, 30687–30720, 2013

31 May for Hangzhou, with 300 $\mu g\,m^{-3}$ for PM_{10} and 220 $\mu g\,m^{-3}$for $PM_{2.5}$, followed by 1 June for Ningbo (PM_{10}: 238 $\mu g\,m^{-3}$; $PM_{2.5}$: 182 $\mu g\,m^{-3}$) and Shanghai (PM_{10}: 208 $\mu g\,m^{-3}$; $PM_{2.5}$: 182 $\mu g\,m^{-3}$), then 2 June for Suzhou, with 271 $\mu g\,m^{-3}$ for PM_{10} and 180 $\mu g\,m^{-3}$for $PM_{2.5}$, and finally 3 June for Nanjing, with 292 $\mu g\,m^{-3}$ for PM_{10} and 217 $\mu g\,m^{-3}$for $PM_{2.5}$, which was consistent with the crop harvest and biomass burning sequence from south to north. Compared with China ambient air quality standards (CAAQS) of 75 $\mu g\,m^{-3}$ for daily $PM_{2.5}$ (Ministry of Environmental Protection of China, 2012), the average and maximum daily concentrations of the episode were 1.1 and 1.9 times for $PM_{2.5}$. The PM concentration level of the episode was comparable with observed results of other biomass burning events in the YRD area. Huang et al. (2012a) observed a pollution episode from 28 May to 3 June in 2009 (almost same as the time period of this study) and measured the average concentrations of $PM_{2.5}$ and PM_{10} of 84 $\mu g\,m^{-3}$ and 136 $\mu g\,m^{-3}$ in Shanghai. During the autumn biomass burning season (14–27 October 2009), Gao et al. (2012) measured the daily average and maximum $PM_{2.5}$ concentrations in Nanjing, which were 200 $\mu g\,m^{-3}$ and 318 $\mu g\,m^{-3}$, respectively. Yin et al. (2011) summarized the official air pollution index (API) of six events in Nanjing during 2006–2009 and found that the corresponding daily maximum PM_{10} concentrations were 338 $\mu g\,m^{-3}$ on 31 May 2006, 375 $\mu g\,m^{-3}$ on 5 June 2007, 218 $\mu g\,m^{-3}$ on 2 June 2008, 350 $\mu g\,m^{-3}$ on 28 October 2008, and 435 $\mu g\,m^{-3}$ on 8 November 2009. Meanwhile, although the crop residues burned in the summer harvest season (mainly straw of wheat and cole flowers) were different from those in autumn (mainly stalks of rice and corn), the PM concentration has no substantial differences.

The daily average concentrations of $PM_{2.5}$ species during the episode are shown in Fig. 3. Organic matters (OM) were the highest value component, accounting for 40.1 % of $PM_{2.5}$ mass. During the episode, daily average and maximum concentrations of OM were 21 and 56 $\mu g\,m^{-3}$ for Shanghai, 25 and 44 $\mu g\,m^{-3}$ for Suzhou, and 39 and 82 $\mu g\,m^{-3}$ for Nanjing. Inorganic ions like sulfate and nitrate were also important $PM_{2.5}$ components. The daily average concentrations were in a range of 10–16 $\mu g\,m^{-3}$

ACPD
13, 30687–30720, 2013

for sulfate, and 10–15 $\mu g\,m^{-3}$ for nitrate. The maximum daily concentrations reached 24 $\mu g\,m^{-3}$ for sulfate and 42 $\mu g\,m^{-3}$ for nitrate. The increase in OM, sulfate and nitrate indicated that the meteorological conditions might have enhanced the formation of secondary aerosols. As a marker of biomass burning, the daily average and maximum concentrations of non-soil K^+ were 1.6 and 5.6 $\mu g\,m^{-3}$ for Shanghai, 2.4 and 5.4 $\mu g\,m^{-3}$ for Suzhou, and 4.9 and 13.6 $\mu g\,m^{-3}$ for Nanjing. The increase in non-soil K^+ concentrations indicated the contribution of biomass burning.

The haze episode can be divided into three phases (see Fig. 2): Phase (I) pre-pollution phase (28 May 0:00–30 May 23:00), Phase (II) pollution phase (31 May 0:00 to 3 June 12:00) and Phase (III) post-pollution phase (3 June 12:00 to 6 June 12:00). For the Nanjing site, Phase II commenced between 2 June 0:00 and 5 June 0:00, one day later than that of other sites. The average concentrations of PM_{10}, $PM_{2.5}$ and key species, and the visual range for each phase were summarized in Table 1. The average PM concentrations increased 1.9–4-fold from Phase I to Phase II. Maximum hourly concentrations during the episode occurred in Phase II, reaching 614 $\mu g\,m^{-3}$ for $PM_{2.5}$ and 660 $\mu g\,m^{-3}$ for PM_{10}. From Phase I to Phase II, the daily average concentrations increased 1.8–3.6-fold for OM and 1–3-fold for EC. Maximum daily OM concentration reached as high as 44–105 $\mu g\,m^{-3}$, accounting for 35–43 % of the $PM_{2.5}$ mass. The increase in OM was the major cause of $PM_{2.5}$ increase. Non-soil K^+ increased most rapidly in Phase II and its maximum daily concentration reached 5.4–18.3 $\mu g\,m^{-3}$, 3.5–15 times that in Phase I. The concentrations of other water-soluble ions also increased in Phase II. Sulfate increased 1.2–2.5-fold, with a maximum daily concentration of 19–20 $\mu g\,m^{-3}$. Nitrate increased 1.3–4.3-fold, and the maximum daily concentration was 19–42 $\mu g\,m^{-3}$ during Phase II.

3.2 Pollution formation and transport

Synoptic weather maps at the surface are given in Fig. 4. The maps show the study region influenced by a ridge on 28 May and in front of a trough after the ridge subse-

ACPD
13, 30687–30720, 2013

quent to 29 May. The continental high pressure moved to the east and entered into the East Sea during this period. From 31 May through 3 June, a tropical depression formed from a low pressure center in the South China Sea, and another low pressure center in northern China was moving south on 31 May. Combined with the influence of three high pressure centers located in the western Pacific Ocean, northern China and southern China, uniform pressure prevailed over most of eastern China. Then the high pressure center in South China moved east and the stagnant weather system under the control of this high pressure lasted until 2 June. At the same time the tropical depression weakened to a low pressure center moving northeast and disappeared on 3 June. The uniform pressure on 1 June was responsible for the transport of air pollutants, while the high pressure on 2 June enhanced the accumulation of pollutants. The weather system in Nanjing, being the furthest west inland, changed one day earlier than other cities as the weather system moved from west to east. From the noon of 3 June, a western wind short-wave trough appeared around the Shanghai area, and there was precipitation during 4–6 June that acted as a cleaning agent, although the thick cloud cover might have reduced mixing depth. The synoptic weather was conducive to pollutant accumulation during Phase II, and clean-out in Phase III.

The temporal variation of relative humidity, visual range, wind speed, precipitation and mixing depth (shown in Figs. 5 and 6) differed among Phases I, II, and III, as shown in Table 2. The major meteorological parameters of the three phases are summarized as follows:

- Phase I (Pre-pollution): There was no precipitation during this period. Average visual range was 6.2–13.9 km with an RH of 50–61 %. Mixing depth was in the range of 458–505 m and wind speed varied between 1.3 and 1.6 $m\,s^{-1}$. The variation in wind speed is consistent with the trend in mixing depth.

- Phase II (Pollution): The precipitation was only 2–5 mm, with RH increased by 5–7 % except for the Nanjing site, with no change in RH as compared to Phase I. The visual range was 3.7–10 km, about 1.2–9.8 km lower than that of Phase I

ACPD
13, 30687–30720, 2013

(shown in Fig. 5). The mixing depth was 240–399 m, 114–218 m lower than that of Phase I. The mixing depth of Nanjing site during this phase was 582 m, which was 93 m higher than that of Phase I. Minimum 3 h mixing depth was as low as 5–30 m. For Shanghai, Nanjing and Ningbo, the wind speeds were 0.2, 0.1 and 0.7 $m s^{-1}$ lower than those of Phase I, respectively. For Suzhou and Hangzhou they were 0.1 and 0.9 $m s^{-1}$ higher than those of Phase I. During the morning of 1 June, the wind speed was above 3 $m s^{-1}$ at Suzhou and Hangzhou (shown in Fig. 6), which benefited the horizontal dispersion of air pollutants and resulted in the temporary reduction of PM concentrations during the late morning of 1 June (see Fig. 2).

– Phase III (Post-pollution): Precipitation was 10–18 mm during this phase, much higher than Phase I and II, except for Nanjing, with precipitation less than 5 mm. Average RH was as high as 77–96 %. Although the PM concentration was quite low, fogs occurred in Nanjing and medium-heavy rain events occurred in other sites, which reduced the visual range (Winkler, 1988; Elias et al., 2009).

Back trajectories along with fire locations and PM_{10} concentrations of two typical days were shown in Fig. 7. MODIS did not detect fires under high cloud cover on 1 June and 5 June (http://modis-atmos.gsfc.nasa.gov/IMAGES), hence 31 May and 4 June were selected to represent Phase II for Nanjing and the four other sites, respectively. On 31 May, fires were mainly located near Hangzhou Bay in northern Zhejiang Province, the southern border of the Shanghai municipality, and southern Jiangsu Province around Tai Lake; only limited fires were found in the area close to Nanjing. For Shanghai, Hangzhou, Ningbo and Suzhou, the main air flow was from the south, mixing with the pollutants from fires along the path. As a result, the main hot spots of PM_{10} pollution concentrated in the area of Shanghai and northern Zhejiang Province, with daily average concentration over 200 $\mu g m^{-3}$. The situation changed on 4 June. Compared with that on 31 May, most fire spots were located in the north, i.e., central Anhui Province and southern Jiangsu Province. The air flow was from the south

ACPD
13, 30687–30720, 2013

for five sites. As a result, high PM_{10} concentration occurred in Jiangsu Province. The daily $PM_{2.5}$ concentrations in Nanjing were between 150 and 290 $\mu g\,m^{-3}$, followed by Suzhou (104 $\mu g\,m^{-3}$). In contrast, the concentrations at the other three sites were all less than 70 $\mu g\,m^{-3}$, and not affected by the biomass burning. With individual monitoring sites, previous studies only reported the possible locations of the biomass burning that affected the air quality in Nanjing. Zhu et al. (2012) found that the pollution of Nanjing was caused by the transport from the north–central area of Jiangsu Province and the northeastern area of Anhui Province on 29 October 2008. Gao et al. (2012) concluded that the source area was in the central area of Jiangsu Province during 14–27 October 2009. Su et al. (2012) found that Nanjing was affected by both Jiangsu Province and Anhui Province on 2 November 2010. Our findings for Nanjing agree with the literature, which is well understood because the crop locations might not have changed and the wind directions are similar during the same periods every year.

3.3 Contributions of biomass burning to particulate pollution

The emission source profiles are crucial for the calculation of receptor modeling such as CMB. Table 2 summarized the mass ratios of $PM_{2.5}$ to K^+, OC to K^+, and EC to K^+ for biomass burning source profiles in the literature. The measured ratios from different studies varied from 4.1 to 175.4 for the $PM_{2.5}/K^+$ ratio, from 0.8 to 121.1 for the OC/K^+ ratio, and from 0.5 to 5.3 for the EC/K^+ ratio. Fuel was one of the dominant factors causing the large variations. However, even with the same burning fuel such as wheat straw, the ratios are still with large ranges, i.e., the $PM_{2.5}/K^+$ ratio varied from 10.1 in China to 4.1 in the US, and the OC/K^+ ratio varied from 3.9 in China to 0.8 in the US. This variability potentially reflects differences in combustion conditions and sampling methods. Cheng et al. (2013) found that the ratio of OC to levoglucosan (another biomass burning marker) also varied between 4.0 and 46.9 due to similar reasons. For the summer harvest period of this study, wheat straw constituted most of the agricultural residues in the YRD region (Yin et al., 2011), and the closest approximation

ACPD
13, 30687–30720, 2013

to these biomass burnings were the measurements by Li et al. (2007), which were conducted in nearby Shandong Province. The mass ratios of $PM_{2.5}/K^+$, OC/K^+ and EC/K^+ used in this study were thus 10.1, 3.9 and 0.8, respectively.

For the WRF/CMAQ model, an important prerequisite was that the model simulation could reproduce the pollution episode well at the base case. Figure 8 compared the modeled and measured hourly $PM_{2.5}$ (TEOM) at each of the five sites, indicating that the CMAQ model gives the same temporal trends and pollution levels as measurements. The normalized mean biases (NMB) were −7 % for Ningbo, −38 % for Hangzhou, −14 % for Shanghai, −9 % for Suzhou and 10 % for Nanjing. However, several outliers from the modeling results were found for the sites of Hangzhou and Ningbo. The simulated pollution peak on 1 June in Hangzhou was much lower than the observed value, which resulted in the model underestimating the measured values by 38 %. For Ningbo, although the NMB was only −7 %, the observed accumulated peak on 1 June was not reproduced. The potential reason for these outliers was the uncertainty of the biomass burning emission spatial distribution under the effect of cloud cover, as the simulated meteorological field and other anthropogenic emissions have been verified at other sites.

The contribution of biomass burning to mass concentrations of $PM_{2.5}$, OC and EC based on the CMAQ model and ambient measurements were compared in Table 3. In general, the model estimates of biomass burning contribution to $PM_{2.5}$ concentrations were comparable with the measurement results, while the modeling results for OC and EC were higher than the measurement results. One of the reasons was that the CMAQ model can include the contribution of primary gaseous precursors of biomass burning to secondary aerosols in $PM_{2.5}$. Another reason was the bias of two different methods and the uncertainties of supporting data. The following discussions are based on the modeling results. Among the five sites, Nanjing was most affected by biomass burning during the episode, followed by Suzhou, Shanghai, Ningbo, and Hangzhou. For the Nanjing site, the contribution of biomass burning was 48 % (64.5 $\mu g\,m^{-3}$) of $PM_{2.5}$, 83 % (29.4 $\mu g\,m^{-3}$) of OC, and 61 % (5.6 $\mu g\,m^{-3}$) of EC. For the Suzhou site,

ACPD
13, 30687–30720, 2013

biomass burning contributed 43 % (49.2 $\mu g\,m^{-3}$) of $PM_{2.5}$, 86 % (28.2 $\mu g\,m^{-3}$) of OC, and 78 % (5.8 $\mu g\,m^{-3}$) of EC. For the Shanghai site, 35 % (28.1 $\mu g\,m^{-3}$) of $PM_{2.5}$, 69 % (15.2 $\mu g\,m^{-3}$) of OC, and 68 % (3.1 $\mu g\,m^{-3}$) of EC were from biomass burning. For the Ningbo site, biomass burning contributed 41 % (30.0 $\mu g\,m^{-3}$) of $PM_{2.5}$, 86 % (18.1 $\mu g\,m^{-3}$) of OC, and 71 % (3.7 $\mu g\,m^{-3}$) of EC. The contribution of biomass burning to $PM_{2.5}$ concentrations in the Hangzhou site was lowest, only 23 %, which might be due to underestimation of the modeling results as shown in Fig. 8.

Based on the WRF/CMAQ modeling results, the contribution of biomass burning in each region was further analyzed, as shown in Fig. 9. It was found that biomass burning of Jiangsu Province and Anhui Province was the major contributor to the Nanjing site, which was consistent with previous studies (Su et al., 2012; Zhu et al., 2012). Jiangsu and Anhui contributed 27 % and 15 % of $PM_{2.5}$ mass concentrations in Nanjing. The widely distributed burning fields in Jiangsu and Anhui Province made Nanjing the most influenced site by biomass burning. Suzhou is located in the center of the YRD region and is mainly affected by the biomass burning from Zhejiang Province and Shanghai municipality. The local biomass burning of Jiangsu Province only contributed 3 % of $PM_{2.5}$ in Suzhou, as Suzhou was located in southern Jiangsu Province and the dominant air flow during the episode was oriented from the south, where Zhejiang Province and Shanghai municipality are located. Shanghai was mainly affected by local biomass burning, which contributed 16 % of $PM_{2.5}$ mass concentrations. The contributions from biomass burning in Zhejiang Province were also important, accounting for 11 % of $PM_{2.5}$ mass. Different from other sites, Ningbo and Hangzhou were mainly affected by local biomass burning in Zhejiang Province. The local burning contributed 37 % and 17 % of $PM_{2.5}$ mass for Ningbo and Hangzhou, respectively.

Overall, the average percentage contribution of biomass burning was 37 % (41 $\mu g\,m^{-3}$) for $PM_{2.5}$, 70 % (19 $\mu g\,m^{-3}$) for OC and 61 % (4 $\mu g\,m^{-3}$) for EC, indicating that biomass burning has significant impacts on this haze episode. The higher contributions of biomass burning to carbonaceous species weakened light efficiently. Although emissions of biomass burning only account for 2.7 % of the annual anthropogenic $PM_{2.5}$

ACPD
13, 30687–30720, 2013

emissions in the YRD region (Huang et al., 2011), it is intensively emitted in a short period after harvest, which rapidly increases $PM_{2.5}$ concentration and decreases visibility, resulting in severe social-economic impacts every year. Furthermore, the contribution of biomass burning from sub-regions further verified that biomass burning could affect both local and regional $PM_{2.5}$ concentrations by atmospheric transport. Regional joint control of biomass burning shall be implemented with efforts and cooperation of all cities.

4 Conclusions

Biomass burning after harvest season could result in severe air pollution and haze issues. In the haze event observed in the summer of 2011, the average and maximum daily $PM_{2.5}$ concentrations reached 82 $\mu g\,m^{-3}$ and 144 $\mu g\,m^{-3}$, respectively. A sharp increase in $PM_{2.5}$, K^+ and carbonaceous aerosol during pollution episodes further confirmed the environmental impact of biomass burning. Stagnant meteorological conditions, caused by a stable high pressure system during 31 May–2 June, combined with high relative humidity and low mixing depth, enhanced the accumulation of air pollutants and caused the formation of haze.

The impacts of biomass open burning on air pollution were quantified using both air quality modeling and measurement methods. It was found that biomass burning contributed 37 % (41 $\mu g\,m^{-3}$) of $PM_{2.5}$, 70 % (19 $\mu g\,m^{-3}$) of OC and 61 % (4 $\mu g\,m^{-3}$) of EC, indicating that biomass burning had significantly affected the air quality in the YRD region. The results of source apportionment also imply that the impact of biomass open burning is regional, due to the substantial inter-province transport of air pollutants. Satellite-detected fire spots, back-trajectory analysis and air model simulation can be integrated to identify the locations where the biomasses are burned. This exercise could be helpful to improve the understanding of heavy pollution episodes.

In addition, this study also has several implications for emission profiles of biomass burning in China. The wide range of $PM_{2.5}$ speciation literature results for biomass

ACPD
13, 30687–30720, 2013

burning emission indicated careful selection of source profiles and encouragement of local field measurement. Although the satellite retrievals such as fire information and aerosol optical depth were powerful for spatial and temporal allocation of biomass burning emissions, the influence of weather factors such as cloud cover and precipitation should be extracted before, especially for the YRD region with high relative humidity.

Supplementary material related to this article is available online at http://www.atmos-chem-phys-discuss.net/13/30687/2013/acpd-13-30687-2013-supplement.pdf.

Acknowledgements. This work is supported by the National Natural Science Foundation of China (21221004& 41227805), MEP's Special Funds for Research on Public Welfares (201009001&2011467003), and the Program for New Century Excellent Talents in University (NCET-10–0532). We acknowledge the support from the local environmental monitoring sites of Nanjing, Suzhou, Pudong, Hangzhou and Ningbo. We also acknowledge the help of L.-W. Antony Chen and Xiaoliang Wang of the Desert Research Institute (Reno, NV, USA), associate professor Haiying Huang of the Shanghai Academy of Environmental Sciences on data analysis, and Chuck Freed from the US EPA on language smoothing.

References

Andreae, M. O. and Merlet, P.: Emission of trace gases and aerosols from biomass burning, Global Biogeochem. Cy., 15, 955–966, doi:10.1029/2000GB001382, 2001.

Cao, J., Wang, Q., Chow, J. C., Watson, J. G., Tie, X., Shen, Z., Wang, P., and An, Z.: Impacts of aerosol compositions on visibility impairment in Xi'an, China, Atmos. Environ., 59, 559–566, doi:10.1016/j.atmosenv.2012.05.036, 2012.

Cao, J., Chow, J. C., Frank, S. C. L., and Watson, J. G.: Evolution of $PM_{2.5}$ measurements and standards in the US and future perspectives for China, Aerosol Air Qual. Res., 13, 1197–1211, doi:10.4209/aaqr.2012.11.0302, 2013.

ACPD
13, 30687–30720, 2013

Cheng, Y., Engling, G., He, K.-B., Duan, F.-K., Ma, Y.-L., Du, Z.-Y., Liu, J.-M., Zheng, M., and Weber, R. J.: Biomass burning contribution to Beijing aerosol, Atmos. Chem. Phys., 13, 7765–7781, doi:10.5194/acp-13-7765-2013, 2013.

Cheng, Z., Chen, C., Huang, C., Huang, H., Li, L., and Wang, H.: Trans-boundary primary air pollution between cities in the Yangtze River Delta, Acta Sci. Circ., 31, 686–694, 2011.

Chow, J. C., Watson, J. G., Pritchett, L. C., Pierson, W. R., Frazier, C. A., and Purcell, R. G.: The dri thermal/optical reflectance carbon analysis system: description, evaluation and applications in US Air quality studies, Atmos. Environ. Part A, Gen. Top., 27, 1185–1201, doi:10.1016/0960-1686(93)90245-T, 1993.

Chow, J. C., Watson, J. G., Robles, J., Wang, X., Chen, L. W. A., Trimble, D., Kohl, S., Tropp, R., and Fung, K.: Quality assurance and quality control for thermal/optical analysis of aerosol samples for organic and elemental carbon, Anal. Bioanal. Chem., 401, 3141–3152, doi:10.1007/s00216-011-5103-3, 2011.

Chow, J. C. and Watson, J. G.: Ion chromatography in elemental analysis of airborne particles, Elem. Anal. Airborne Part., 1, 97–137, 1999.

Chow, J. C., Engelbrecht, J. P., Watson, J. G., Wilson, W. E., Frank, N. H., and Zhu, T.: Designing monitoring networks to represent outdoor human exposure, Chemosphere, 49, 961–978, doi:10.1016/S0045-6535(02)00239-4, 2002.

Chow, J. C., Watson, J. G., Chen, L. W. A., Chang, M. C. O., Robinson, N. F., Trimble, D., and Kohl, S.: The IMPROVE_A temperature protocol for thermal/optical carbon analysis: maintaining consistency with a long-term database, J. Air Waste Manage., 57, 1014–1023, doi:10.3155/1047-3289.57.9.1014, 2007.

Chow, J. C., Doraiswamy, P., Watson, J. G., Antony-Chen, L. W., Ho, S. S. H., and Sodeman, D. A.: Advances in integrated and continuous measurements for particle mass and chemical, composition, J. Air Waste Manage., 58, 141–163, doi:10.3155/1047-3289.58.2.141, 2008.

Crutzen, P. J. and Andreae, M. O.: Biomass burning in the tropics: impact on atmospheric chemistry and biogeochemical cycles, Science, 250, 1669–1678, doi:10.1126/science.250.4988.1669, 1990.

Davies, D. K., Ilavajhala, S., Wong, M. M., and Justice, C. O.: Fire information for resource management system: archiving and distributing MODIS active fire data, IEEE T. Geosci. Remote Sens., 47, 72–79, 2009.

ACPD
13, 30687–30720, 2013

Draxler, R. R. and Rolph, G. D.: HYSPLIT (HYbrid Single-Particle Lagrangian Integrated Trajectory) Model access via NOAA ARL READY Website: http://ready.arl.noaa.gov/HYSPLIT.php, NOAA Air Resources Laboratory, Silver Spring, MD, 2013.

Duan, F. K., Liu, X. D., Yu, T., and Cachier, H.: Identification and estimate of biomass burning contribution to the urban aerosol organic carbon concentrations in Beijing, Atmos. Environ., 38, 1275–1282, doi:10.1016/j.atmosenv.2003.11.037, 2004.

Elias, T., Haeffelin, M., Drobinski, P., Gomes, L., Rangognio, J., Bergot, T., Chazette, P., Raut, J. C., and Colomb, M.: Particulate contribution to extinction of visible radiation: pollution, haze, and fog, Atmos. Res., 92, 443–454, 2009.

Fu, X., Wang, S., Zhao, B., Xing, J., Cheng, Z., Liu, H., and Hao, J.: Emission inventory of primary pollutants and chemical speciation in 2010 for the Yangtze River Delta region, China, Atmos. Environ., 70, 39–50, doi:10.1016/j.atmosenv.2012.12.034, 2013.

Gao, C., Wang, T., Wu, J., Fei, Q., and Cao, L.: Study on a continuous haze weather event during autumn of 2009 in Nanjing, Sci. Meteorol. Sin., 32, 246–252, 2012.

Gelencsér, A., May, B., Simpson, D., Sánchez-Ochoa, A., Kasper-Giebl, A., Puxbaum, H., Caseiro, A., Pio, C., and Legrand, M.: Source apportionment of $PM_{2.5}$ organic aerosol over Europe: primary/secondary, natural/anthropogenic, and fossil/biogenic origin, J. Geophys. Res.-Atmos., 112, D23S04, doi:10.1029/2006JD008094, 2007.

Guenther, A., Karl, T., Harley, P., Wiedinmyer, C., Palmer, P. I., and Geron, C.: Estimates of global terrestrial isoprene emissions using MEGAN (Model of Emissions of Gases and Aerosols from Nature), Atmos. Chem. Phys., 6, 3181–3210, doi:10.5194/acp-6-3181-2006, 2006.

Hand, J. L.: Spatial and Seasonal Patterns and Temporal Variability of Haze and its Constituents in the United States, Cooperative Institute for Research in the Atmosphere (CIRA), Colorado State University, 2011.

Hays, M. D., Fine, P. M., Geron, C. D., Kleeman, M. J., and Gullett, B. K.: Open burning of agricultural biomass: physical and chemical properties of particle-phase emissions, Atmos. Environ., 39, 6747–6764, doi:10.1016/j.atmosenv.2005.07.072, 2005.

Hidy, G. M., Chow, J. C., England, G. C., Legge, A. H., Lloyd, A. C., and Watson, J. G.: Energy supplies and future engines for land, sea, and air, J. Air Waste Manage., 62, 1233–1248, 2012.

Huang, C., Chen, C. H., Li, L., Cheng, Z., Wang, H. L., Huang, H. Y., Streets, D. G., Wang, Y. J., Zhang, G. F., and Chen, Y. R.: Emission inventory of anthropogenic air pollutants and VOC

ACPD
13, 30687–30720, 2013

species in the Yangtze River Delta region, China, Atmos. Chem. Phys., 11, 4105–4120, doi:10.5194/acp-11-4105-2011, 2011.
Huang, K., Zhuang, G., Lin, Y., Fu, J. S., Wang, Q., Liu, T., Zhang, R., Jiang, Y., Deng, C., Fu, Q., Hsu, N. C., and Cao, B.: Typical types and formation mechanisms of haze in an Eastern Asia megacity, Shanghai, Atmos. Chem. Phys., 12, 105–124, doi:10.5194/acp-12-105-2012, 2012a.
Huang, X.-F., He, L.-Y., Xue, L., Sun, T.-L., Zeng, L.-W., Gong, Z.-H., Hu, M., and Zhu, T.: Highly time-resolved chemical characterization of atmospheric fine particles during 2010 Shanghai World Expo, Atmos. Chem. Phys., 12, 4897–4907, doi:10.5194/acp-12-4897-2012, 2012b.
Li, W. J., Shao, L. Y., and Buseck, P. R.: Haze types in Beijing and the influence of agricultural biomass burning, Atmos. Chem. Phys., 10, 8119–8130, doi:10.5194/acp-10-8119-2010, 2010.
Li, X., Wang, S., Duan, L., Hao, J., Li, C., Chen, Y., and Yang, L.: Particulate and Trace Gas Emissions from Open Burning of Wheat Straw and Corn Stover in China, Environ. Sci. Technol., 41, 6052–6058, doi:10.1021/es0705137, 2007.
Lowenthal, D. and Kumar, N.: $PM_{2.5}$ mass and light extinction reconstruction in IMPROVE, J. Air Waste Manage., 53, 1109–1120, doi:10.1080/10473289.2003.10466264, 2003.
Penner, J. E., Dickinson, R. E., and Oneill, C. A.: Effects of aerosol from biomass burning on the global radiation budget, Science, 256, 1432–1434, doi:10.1126/science.256.5062.1432, 1992.
Reisen, F., Meyer, C. P., and Keywood, M. D.: Impact of biomass burning sources on seasonal aerosol air quality, Atmos. Environ., 67, 437–447, doi:10.1016/j.atmosenv.2012.11.004, 2013.
Rolph, G. D.: Real-time Environmental Applications and Display System (READY) Website: http://ready.arl.noaa.gov, NOAA Air Resources Laboratory, Silver Spring, MD, 2013.
Sheesley, R. J., Schauer, J. J., Chowdhury, Z., Cass, G. R., and Simoneit, B. R. T.: Characterization of organic aerosols emitted from the combustion of biomass indigenous to South Asia, J. Geophys. Res., 108, 4285, doi:10.1029/2002jd002981, 2003.
Song, Y., Tang, X., Xie, S., Zhang, Y., Wei, Y., Zhang, M., Zeng, L., and Lu, S.: Source apportionment of $PM_{2.5}$ in Beijing in 2004, J. Hazard. Mater., 146, 124–130, doi:10.1016/j.jhazmat.2006.11.058, 2007.

ACPD
13, 30687–30720, 2013

SPECIATE4.3: Agricultural Burning – Composite: http://cfpub.epa.gov/si/speciate/ehpa_speciate_browse_details.cfm?ptype=P&pnumber=91103, SPECIATE 4.3, United States, 2009.

Streets, D. G., Yarber, K. F., Woo, J. H., and Carmichael G. R.: Biomass burning in Asia: Annual and seasonal estimates and atmospheric emissions, Global Biogeochem. Cy., 17, 1099, doi:10.1029/2003GB002040, 2003.

Su, J.-F., Zhu, B., Zhou, T., and Ren, Y.-B.: Contrast analysis of two serious air pollution events affecting Nanjing and its surrounding regions resulting from burning of crop residues, J. Ecol. Rural Environ., 28, 37–41, 2012.

Sullivan, A. P., Holden, A. S., Patterson, L. A., McMeeking, G. R., Kreidenweis, S. M., Malm, W. C., Hao, W. M., Wold, C. E., and Collett, J. L.: A method for smoke marker measurements and its potential application for determining the contribution of biomass burning from wildfires and prescribed fires to ambient $PM_{2.5}$ organic carbon, J. Geophys. Res., 113, D22302, doi:10.1029/2008jd010216, 2008.

Tian, D., Hu, Y., Wang, Y., Boylan, J. W., Zheng, M., and Russell, A. G.: Assessment of biomass burning emissions and their impacts on urban and regional $PM_{2.5}$: a georgia case study, Environ. Sci. Technol., 43, 299–305, doi:10.1021/es801827s, 2008.

Wang, Q., Shao, M., Liu, Y., William, K., Paul, G., Li, X., Liu, Y., and Lu, S.: Impact of biomass burning on urban air quality estimated by organic tracers: Guangzhou and Beijing as cases, Atmos. Environ., 41, 8380–8390, doi:10.1016/j.atmosenv.2007.06.048, 2007.

Wang, Q., Shao, M., Zhang, Y., Wei, Y., Hu, M., and Guo, S.: Source apportionment of fine organic aerosols in Beijing, Atmos. Chem. Phys., 9, 8573–8585, doi:10.5194/acp-9-8573-2009, 2009.

Wang, S., Xing, J., Chatani, S., Hao, J., Klimont, Z., Cofala, J., and Amann, M.: Verification of anthropogenic emissions of China by satellite and ground observations, Atmos. Environ., 45, 6347–6358, doi:10.1016/j.atmosenv.2011.08.054, 2011a.

Wang, Y., Hopke, P. K., Rattigan, O. V., Xia, X., Chalupa, D. C., and Utell, M. J.: Characterization of residential wood combustion particles using the two-wavelength aethalometer, Environ. Sci. Technol., 45, 7387–7393, doi:10.1021/es2013984, 2011b.

Watson, J. G.: Visibility: science and regulation, J. Air Waste Manage., 52, 628–713, 2002.

Watson, J. G., Antony Chen, L.-W., Chow, J. C., Doraiswamy, P., and Lowenthal, D. H.: Source apportionment: findings from the US Supersites Program, J. Air Waste Manage., 58, 265–288, 2008.

ACPD
13, 30687–30720, 2013

Winkler, P.: The growth of atmospheric aerosol particles with relative humidity, Phys. Scripta, 37, 223, 1988.
Yan, X., Ohara, T., and Akimoto, H.: Bottom-up estimate of biomass burning in mainland China, Atmos. Environ., 40, 5262–5273, doi:10.1016/j.atmosenv.2006.04.040, 2006.
Yang, F., Tan, J., Zhao, Q., Du, Z., He, K., Ma, Y., Duan, F., Chen, G., and Zhao, Q.: Characteristics of $PM_{2.5}$ speciation in representative megacities and across China, Atmos. Chem. Phys., 11, 5207–5219, doi:10.5194/acp-11-5207-2011, 2011.
Yin, C., Zhu, B., Cao, Y.-C., Su, J.-F., Wang, X.-Y., and Wang, H.: The origin of crop residue burning impact on air quality of Nanjing, China Environ. Sci., 31, 207–213, 2011.
Zhang, X., Hecobian, A., Zheng, M., Frank, N. H., and Weber, R. J.: Biomass burning impact on $PM_{2.5}$ over the southeastern US during 2007: integrating chemically speciated FRM filter measurements, MODIS fire counts and PMF analysis, Atmos. Chem. Phys., 10, 6839–6853, doi:10.5194/acp-10-6839-2010, 2010a.
Zhang, Y., Duan, Y., Gao, S., Wei, H., Sha, F., Cai, Y., and Shen, L.: Characteristics of fine particulate matter during a typical air pollution episode in Shanghai urban area, China Environ. Sci., 31, 1115–1121, 2011.
Zhang, Z., Engling, G., Lin, C.-Y., Chou, C. C. K., Lung, S.-C. C., Chang, S.-Y., Fan, S., Chan, C.-Y., and Zhang, Y.-H.: Chemical speciation, transport and contribution of biomass burning smoke to ambient aerosol in Guangzhou, a mega city of China, Atmos. Environ., 44, 3187–3195, doi:10.1016/j.atmosenv.2010.05.024, 2010b.
Zhu, B., Su, J., Han, Z., Yin, C., and Wang, T.: Analysis of a serious air pollution event resulting from crop residue burning over Nanjing and surrounding regions, China Environ. Sci., 30, 585–592, 2010.
Zhu, J., Wang, T., Xing, L., Mu, Q., and Zhou, D.: Analysis on the characteristics and mechanism of a heavy haze episode in Jiangsu Province, China Environ. Sci., 31, 1943–1950, 2011.
Zhu, J., Wang, T., Deng, J., Jiang, A., and Liu, D.: An emission inventory of air pollutants from crop residue burning in Yangtze River Delta Region and its application in simulation of a heavy haze weather process, Acta Sci. Circ., 32, 3045–3055, 2012.

ACPD
13, 30687–30720, 2013

Table 1. PM concentration, visual range and meteorological parameters for three phases of the pollution episode.

Index	Phase*	Sampling Sites Ningbo	Hangzhou	Shanghai	Suzhou	Nanjing
PM mass ($\mu g m^{-3}$)	I	PM_{10}: 91, $PM_{2.5}$: 51	PM_{10}: 115, $PM_{2.5}$: 64	PM_{10}: 60, $PM_{2.5}$: 37	PM_{10}: $PM_{2.5}$: 109, 55	PM_{10}: 114, $PM_{2.5}$: 60
	II	PM_{10}: 176, $PM_{2.5}$: 125	PM_{10}: 225, $PM_{2.5}$: 157	PM_{10}: 160, $PM_{2.5}$: 128	PM_{10}: $PM_{2.5}$: 220,139	PM_{10}: 240, $PM_{2.5}$: 180
	III	PM_{10}: 41, $PM_{2.5}$: 32	PM_{10}: 58, $PM_{2.5}$: 41	PM_{10}: 28, $PM_{2.5}$: 25	PM_{10}: $PM_{2.5}$: 73, 40	PM_{10}: 99, $PM_{2.5}$: 64
$PM_{2.5}$ species ($\mu g m^{-3}$)	I	N/A	N/A	K^+: 0.3, OM: 12, EC: 2	K^+: 1.5, OM: 23, EC: 4	K^+: 3.2, OM: 31, EC: 5
	II	N/A	N/A	K^+: 4.5, OM: 43, EC: 6	K^+: 5.3, OM: 42, EC: 4	K^+: 14, OM: 82, EC: 10
	III	N/A	N/A	K^+: 0.6, OM: 10, EC: 2	K^+: 1.7, OM: 16, EC: 3	K^+: 3.5, OM: 35, EC: 4
Visual range (km)	I	13.9	6.2	13.5	8.5	11.0
	II	10.0	5.0	3.7	3.8	5.4
	III	10.4	4.9	8.7	4.9	4.2
RH (%)	I	58	59	56	56	50
	II	65	65	61	61	50
	III	84	96	79	78	77
Mixing depth (m)	I	458	505	461	541	489
	II	240	391	295	399	582
	III	248	283	319	405	627
Wind speed ($m s^{-1}$)	I	1.6	1.6	1.3	1.3	1.5
	II	0.9	2.5	1.1	1.4	1.4
	III	0.9	1.2	1.4	1.4	1.9

* Pre-pollution phase (28 May 00:00 to 30 May 23:00, marked I), pollution phase (31 May 00:00 to 3 June 12:00, marked II) and post-pollution phase (3 June 12:00 to 6 June 12:00, marked III). For the Nanjing site, pre-pollution phase (28 May 00:00 to 1 June 23:00, marked I), pollution phase (2 June 00:00 to 4 June 23:00, marked II) and post-pollution phase (5 June 00:00 to 6 June 12:00, marked III).

ACPD
13, 30687–30720, 2013

Table 2. Mass ratio of $PM_{2.5}$, OC and EC, normalized to water soluble potassium (K^+) in the literature.

Observation	Biomass type	Location	Mass ratio	Reference
$PM_{2.5}/K^+$	Wheat straw	Shandong, China	10.1*	Li et al. (2007)
		Washington, US	4.07	Hays et al. (2005)
	Rice straw	South Asia	50	Sheesley et al. (2003)
		Washington, US	175.4	Hays et al. (2005)
	Maize stover	Shandong, China	11.8	Li et al. (2007)
	Agricultural residues	California, US	14.2	SPECIATE4.3 (2009)
		Global average	9.1–30	Andreae and Merlet (2001)
OC/K^+	Wheat straw	Shandong, China	3.9*	Li et al. (2007)
		Washington, US	0.8	Hays et al. (2005)
	Rice straw	South Asia	26.3	Sheesley et al. (2003)
		Washington, US	121.1	Hays et al. (2005)
	Maize stover	Shandong, China	3.9	Li et al. (2007)
	Agricultural residues	California, US	5.5	SPECIATE4.3 (2009)
		Global average	7.7–25.8	Andreae and Merlet (2001)
EC/K^+	Wheat straw	Shandong, China	0.8*	Li et al. (2007)
		Washington, US	0.5	Hays et al. (2005)
	Rice straw	South Asia	1.6	Sheesley et al. (2003)
		Washington, US	2.3	Hays et al. (2005)
	Maize stover	Shandong, China	0.4	Li et al. (2007)
	Agricultural residues	California, US	1.6	SPECIATE4.3 (2009)
		Global average	1.6–5.3	Andreae and Merlet (2001)

* The value used in this study.

ACPD
13, 30687–30720, 2013

Table 3. Contribution of biomass burning to mass concentrations of $PM_{2.5}$, OC and EC.

Site	Method	$PM_{2.5}$ (Average±SD)		OC (Average±SD)		EC(Average±SD)	
		Value ($\mu g\,m^{-3}$)	Ratio[b] (%)	Value ($\mu g\,m^{-3}$)	Ratio[b] (%)	Value ($\mu g\,m^{-3}$)	Ratio[b] (%)
Ningbo[a]	WRF/CMAQ	30.0±8.0	41 ± 5	18.1 ± 4.1	86 ± 5	3.7 ± 0.9	71 ± 9
Hangzhou[a]	WRF/CMAQ	17.6 ± 16.5	23 ± 13	7.8 ± 8.8	56 ± 28	1.5 ± 1.8	38 ± 26
Shanghai	Measurement	29.2 ± 23.4	26 ± 15	10.4 ± 8.3	48 ± 26	2.1 ± 1.7	44 ± 27
	WRF/CMAQ	28.1 ± 10.4	35 ± 5	15.2 ± 4.5	69 ± 8	3.1 ± 0.9	68 ± 9
Suzhou	Measurement	35.7 ± 21.2	30 ± 13	12.7 ± 7.5	60 ± 22	2.5 ± 1.5	56 ± 35
	WRF/CMAQ	49.2 ± 28.0	43 ± 8	28.2 ± 14.5	86 ± 7	5.8 ± 3.0	78 ± 9
Nanjing	Measurement	74.9 ± 48.4	47 ± 19	26.6 ± 17.2	71 ± 16	5.3 ± 3.4	70 ± 22
	WRF/CMAQ	64.5 ± 26.7	48 ± 8	29.4 ± 13.3	83 ± 7	5.6 ± 2.8	61 ± 13
Average	–	41.2	37	18.6	70	3.7	61

[a] The sites of Hangzhou and Ningbo have no measurement results due to sampling instrument absence.

[b] For the measurement method, the ratio is calculated by the biomass burning contributed concentration normalized the measured ambient concentration; for the WRF/CMAQ method, the ratio is calculated by the biomass burning contributed concentration normalized the simulated ambient concentration under the base case.

ACPD
13, 30687–30720, 2013

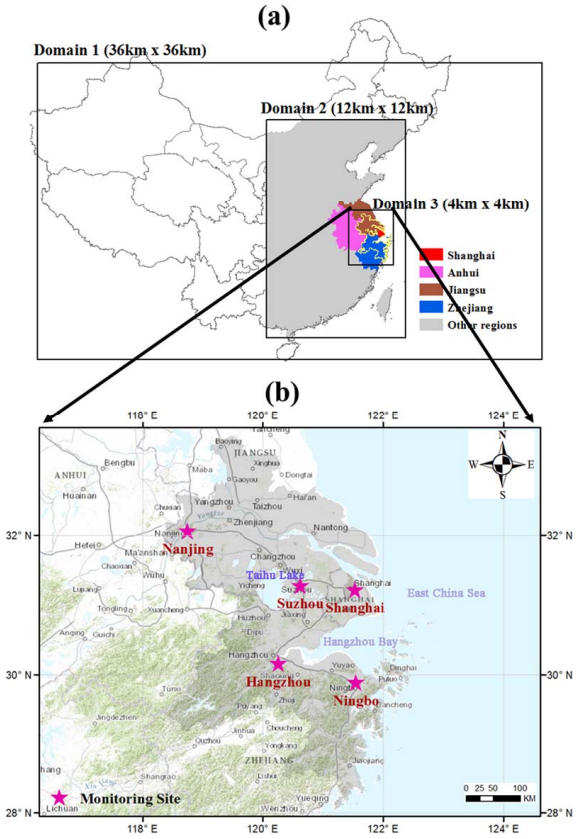

Fig. 1. Model domain and location of measurement sites. **(a)** Three nested domain grids for WRF/CMAQ modeling. **(b)** Location of field monitoring sites. The yellow border in **(a)** and gray area in **(b)** constitute the YRD region. The five regions indicated by different colors in panel **(a)** were used for WRF/CMAQ sensitivity analyses, with biomass burning emissions set to zero in each region to determine their effects on concentrations of $PM_{2.5}$ and carbon species.

ACPD
13, 30687–30720, 2013

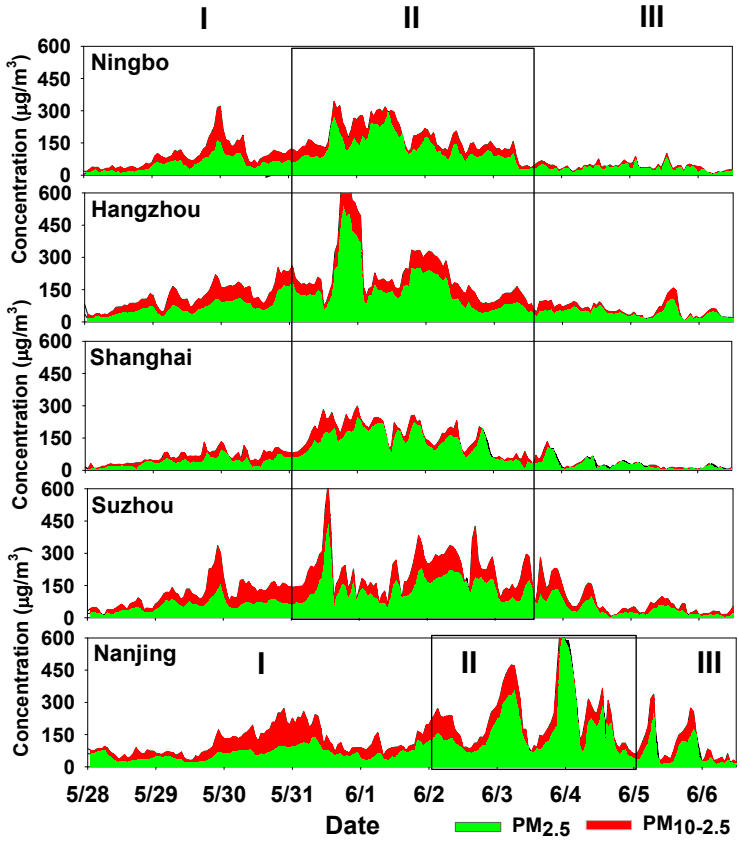

Fig. 2. Evolution of TEOM $PM_{2.5}$ (green) and $PM_{10-2.5}$ (red) mass concentrations during the monitoring period. The black lines show different phases described in the text.

ACPD
13, 30687–30720, 2013

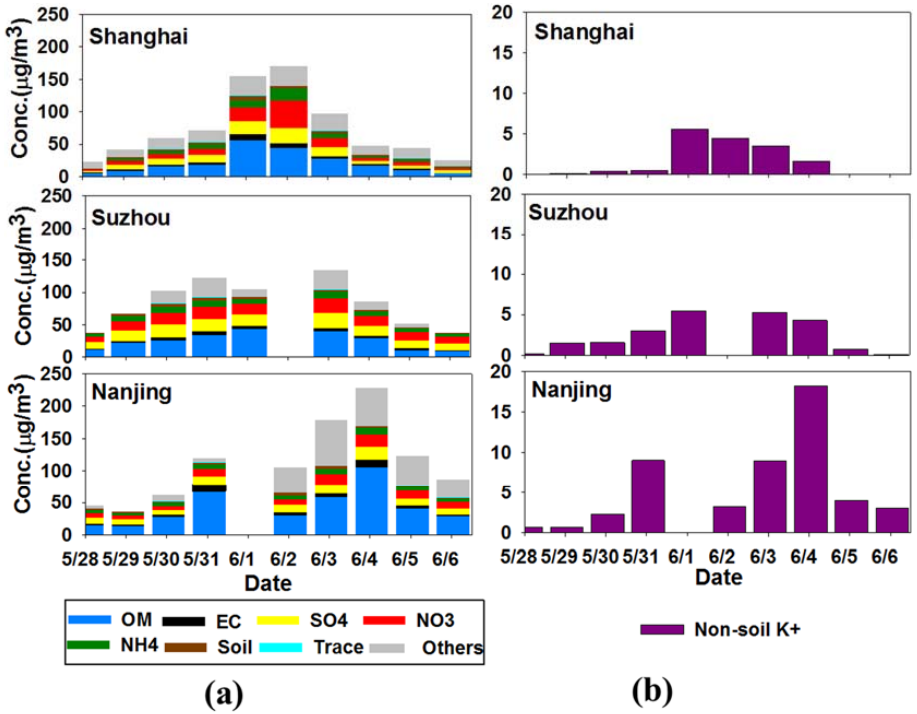

Fig. 3. (a) Daily average concentrations of $PM_{2.5}$ with chemical components. **(b)** Concentrations of non-soil soluble potassium (K^+) in $PM_{2.5}$. Organic Matter (OM) = 1.55OC, Soil = 2.2Al + 2.49Si + 1.63Ca + 2.42Fe + 1.94Ti, Trace = As + Br + Cr + Cu + Mn + Ni + Pb + Rb + Se + Sr + Zn, Non-soil $K^+ = K^+ - 0.6Fe$, Others = $PM_{2.5}$ mass – (OM + EC + SO_4 + NO_3 + NH_4 + Soil + Trace + Non-soil K^+). No data available for Hangzhou and Ningbo.

ACPD
13, 30687–30720, 2013

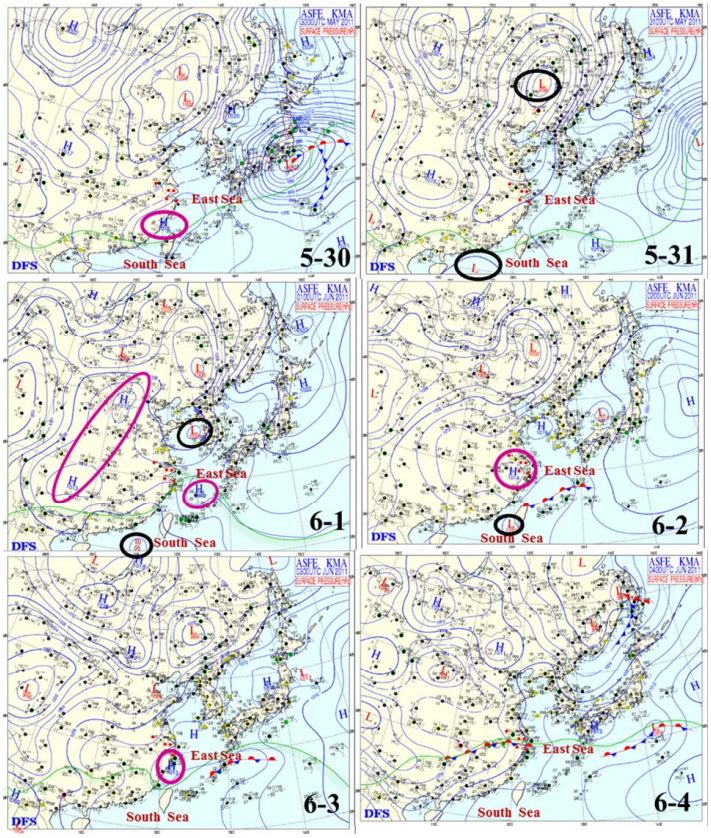

Fig. 4. Surface weather patterns over eastern China from 30 May to 4 June 2011. Black circle represents the low pressure center, pink circle represents the high pressure center, and red dot denotes the sampling site.

ACPD
13, 30687–30720, 2013

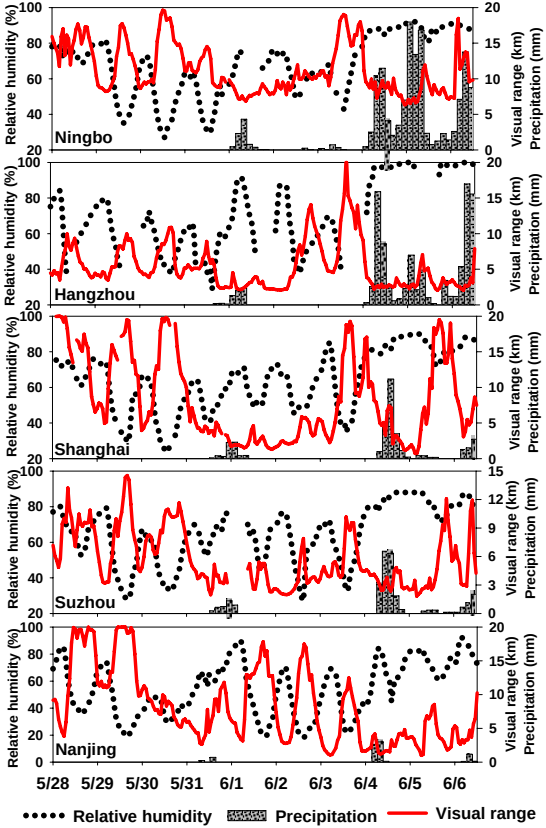

Fig. 5. Relative humidity (black dots), visual range (red line) and precipitation (shaded bar) at each site from 28 May through 6 June 2011.

ACPD
13, 30687–30720, 2013

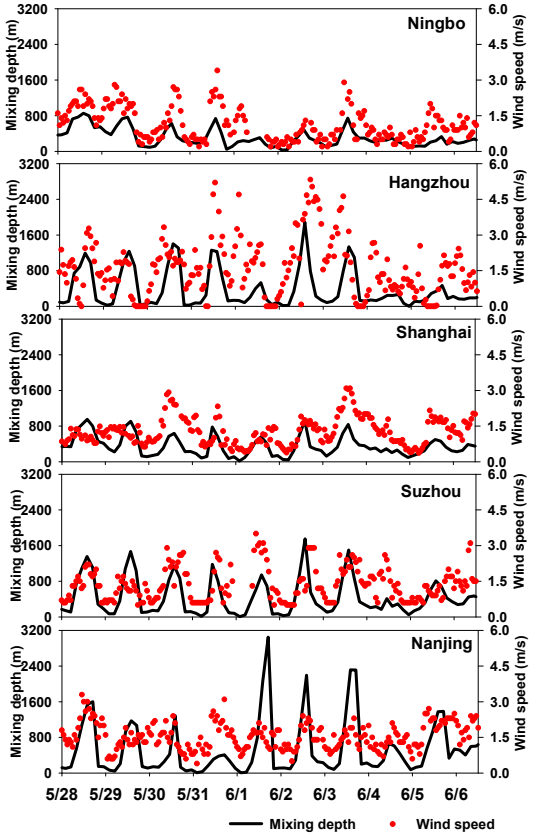

Fig. 6. Mixing depths (black lines) and wind speeds (red dots) at each monitoring site from 28 May through 6 June 2011.

ACPD
13, 30687–30720, 2013

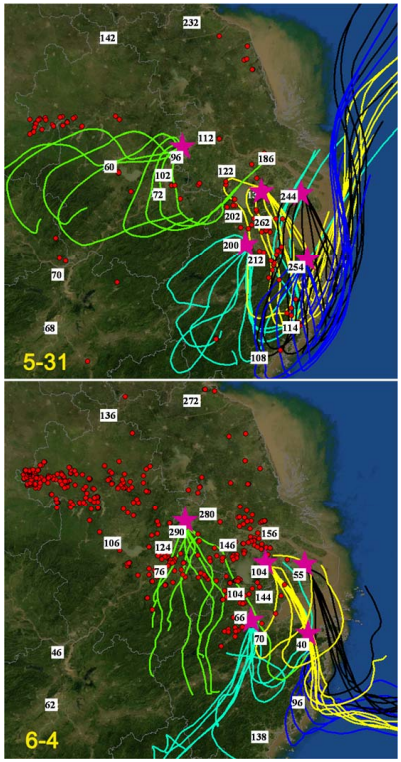

Fig. 7. HYSPLIT 24 h back-trajectories at 100 m a.g.l. originating at each monitoring site (purple stars), calculated every 3 h beginning at 12:00 LST and ending at 09:00 LST the following day. Red dots represent the satellite-detected fires (FIRMS, Davies et al., 2009). Numbers are the daily average PM_{10} mass concentrations from air quality monitoring (http://datacenter.mep.gov.cn/report/air_daily/air_dairy.jsp). Back-trajectory colors are: Black-Shanghai, Blue-Ningbo, Cyan-Hangzhou, Yellow-Suzhou, Green-Nanjing.

ACPD
13, 30687–30720, 2013

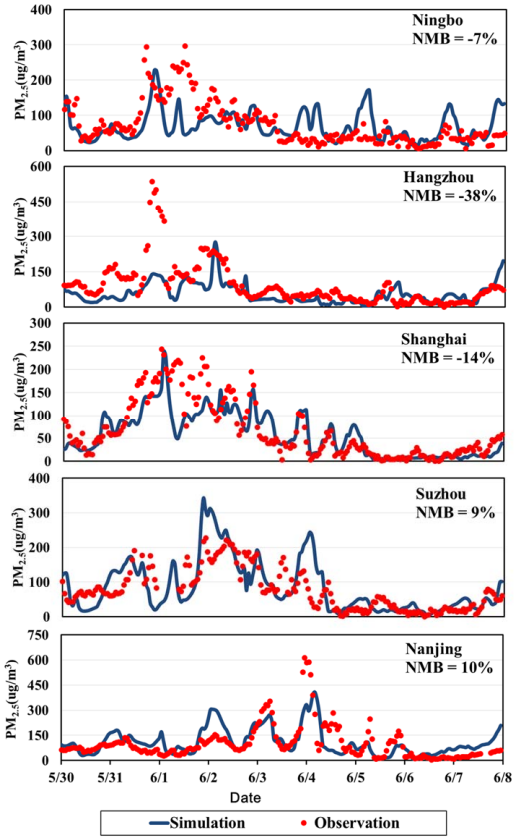

Fig. 8. Comparison of CMAQ simulations (blue lines) and TEOM-measured (red dots) hourly $PM_{2.5}$ mass concentrations. NMB means normalized mean bias.

ACPD
13, 30687–30720, 2013

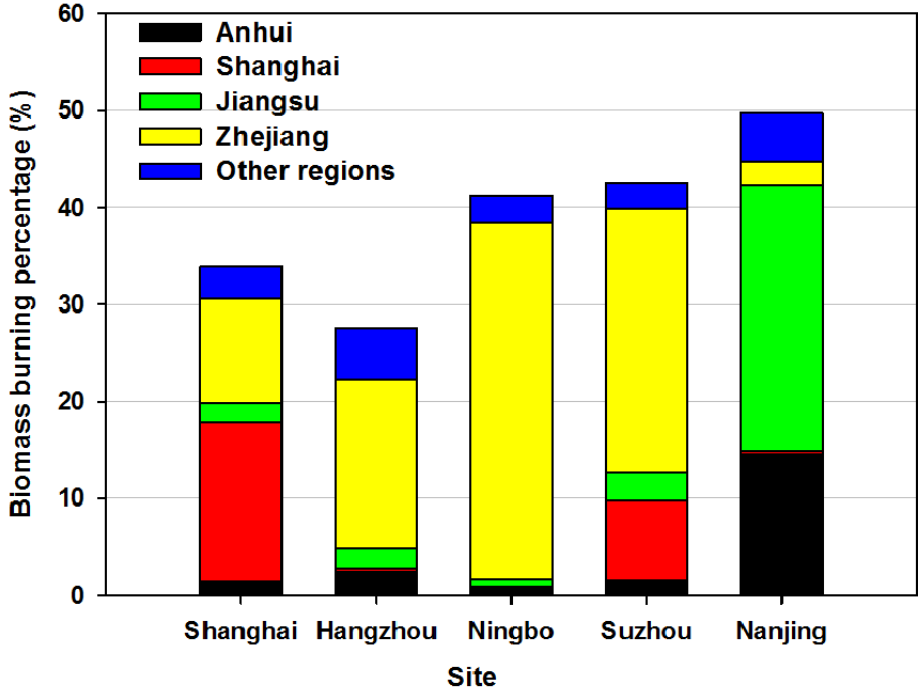

Fig. 9. Percentage contribution of biomass burning to $PM_{2.5}$ mass concentration. Location of each region is shown in Fig. 1. The remaining percentage represents the contribution of other emission sources.

ACPD
13, 30687–30720, 2013